Comparison of linear and nonlinear optical properties of ZnO nanorods

Susanta Kumar Das[1,4], Frank Güell[2], Ciarán Gray[3], Daragh Byrne[3], Prasanta Kumar Das[4], Ruediger Grunwald[1], Günter Steinmeyer[1], and Enda McGlynn[3],*

[1]*Max-Born-Institut für Nichtlineare Optik und Kurzzeitspektroskopie, Max-Born-Strasse 2a, D-12489 Berlin, Germany.*

[2]*Departament d'Electrònica, Universitat de Barcelona, C/Martí i Franquès 1, E-08028 Barcelona, Catalunya, Spain.*

[3]*School of Physical Sciences, National Centre for Plasma Science and Technology, Dublin City University, Glasnevin, Dublin 9, Ireland.*

[4]*School of Applied Sciences, KIIT University, Bhubaneswar - 751024, Odisha, India.*

*enda.mcglynn@dcu.ie

1.1 Introduction

ZnO nanostructures display an exceptional range of nanomorphologies and can be synthesised by a wide range of growth methods. Materials grown in various morphologies by different growth methods have differing advantages and disadvantages from the point of view of applications.[1] As one example, ZnO synthesised at higher temperatures using vapour phase transport (VPT) results in deposited material with excellent optical emission, but deposition is generally over limited areas, whereas ZnO synthesised at lower temperatures using chemical bath deposition (CBD) results in material with characteristically poor optical properties such as photoluminescence (PL) emission but the growth method allows uniform deposition over large areas.[2,3]

Furthermore, the many promising qualities of ZnO mean that researchers wish to utilise a diverse range of substrates, including flexible plastic substrates. It is generally unfeasible to employ growth temperatures > 400^0C with plastic substrates without causing significant substrate damage or destruction. This issue has further spurred the interest of researchers in terms of the development of low temperature (< 400^0C and even in some cases < 100^0C) CBD methods.[4] ZnO nanostructures grown by such CBD methods show a range of morphologies but in many cases they yield well-aligned arrays of close-packed nanorods with diameters ~ 50 – 300 nm, regardless of the substrates type, dominated by crystal facet energetics and proximity effects.[4–6]

In all cases known to the authors, while the structural properties of both VPT- and CBD-grown ZnO nanorods are comparably good and single crystal nanostructures are reported, the linear optical properties, specifically PL emission, are significantly worse for CBD-grown nanostructures compared to VPT-grown material. This is evidenced in a variety of ways in the PL such as (i) generally strong defect band to the bandedge emission ratio, (ii) generally far weaker PL emissions, and, very importantly (iii) very large low temperature PL

bound exciton linewidths (~ 10 meV).[7] While the linear optical properties such as PL emission intensity can be somewhat improved by annealing, the linewidths do not improve to anything close to the values (< 1 meV) seen in PL from nanostructures grown by VPT.[8] Trade-offs of this nature between linear optical properties and deposition area and scalability are generally found in the different growth methods of ZnO nanostructures, and their origins seem fundamentally linked to the key advantage of the CBD methods, low temperature synthesis. Thus it is difficult to envisage solutions to this problem for linear optical properties, since techniques such as annealing (which is at best only partially successful in improving the PL emission properties) themselves will lead to problems as those observed for high temperature growth methods due to the high temperatures involved.

By contrast, the nonlinear properties of these nanomaterials, including third order nonlinearities, and the variation of these properties as a consequence of different growth methods, are less widely reported. For example, there is a limited number of reports of third harmonic generation (THG) from ZnO nanomaterials, whereas a greater number of publications deal with second harmonic generation (SHG) from ZnO and ZnO nanostructures.[9–12] Frequency conversion and other nonlinear phenomena in ZnO nanostructures are of importance because many application areas might benefit from UV generation via THG. For example ultrashort fs laser pulse characterization is rendered challenging due to their broadband spectrum (> 100 nm) which means that dispersive effects can dominate, and this in turn typically requires a sub-20 μm material path for sufficiently broadband phase matching. Thus, one requires very thin nonlinear crystals for this type of application.[13] There have been recent reports of thin nanocrystalline TiO_2 films used for pulses down to 20 fs, which effectively demonstrates the proof of principle that for nano length scale deposits the normal phase-matching constraints associated with traditional bulk nonlinear materials are relaxed.[14] In terms of an application in a very different technology space, efficient UV delivery to sites inside the human body, either by coupling NIR radiation into the body via the "optical tissue window" wavelengths (0.7–1.1 μm) and then upconverting to UV, or using waveguides to couple NIR radiation to nanostructures embedded in tissue, and again upconverting to UV, may allow the advancement of new methods of spatially localised UV photodynamic therapy, down to the size of single cells.[15–19] Indeed CBD-grown ZnO nanorods have been used to make measurements within a cell.[19] However these types of applications all rely on high UV conversion efficiencies.

In this chapter PL emission and THG by both CBD-grown and VPT-grown ZnO nanorod samples are reported. These studies clearly show that the low temperature PL emission from CBD-grown samples is both weaker in intensity and broader in terms of key feature linewidths than that from VPT-grown samples. By contrast the THG efficiency of samples grown by both the high temperature and low temperature methods are comparable to one another, and both are much larger than THG generated at a bare quartz surface. Intensity dependence measurement and interferometric frequency resolved optical gating (iFROG) measurements are used to study the THG from both sample types.[20,21] The laser pulse parameters are extracted when the pulses are subjected to both high and low chirp and our studies indicate that ZnO nanostructures grown by low temperature methods allow excellent

characterization of ultrafast pulses (originally < 10 fs) and can efficiently generate THG. Consequently ZnO nanostructures grown by low temperature methods are excellent candidate materials for the technology applications discussed above.

2.1 Experimental details

2.1.1 ZnO nanostructure growth and structural characterization

ZnO nanostructures were grown by both CBD (on fused silica substrates and Si (111) or Si (100) substrates) and by VPT (on (11-20) sapphire substrates and Si (111) or Si (100) substrates).

2.1.1.1 CBD growth

The details of the growth method employed for CBD have been given elsewhere.[2,22,23] In summary, substrates cleaned by sonication in acetone and ethanol were dried in a nitrogen stream and then coated with a ZnO seed layer via drop coating. Typically the drop coated seed layer was prepared by applying 3.75 μl per cm^2 of substrate of a 5 mM zinc acetate in absolute ethanol solution for 20 seconds before a rinse with absolute ethanol and drying the sample with a nitrogen stream. Drop coating was normally repeated four more times and samples were annealed at 350^0C in air for 30 min. ZnO nanorods were deposited on the seeded substrates using a 0.02 M zinc nitrate solution added slowly to an equal volume of 0.8 M NaOH solution with vigorous stirring. This solution was heated to 70^0C and the substrates were then immersed in it, maintaining the temperature for 25 min, with gentle stirring. The substrates were then removed from the solution, washed with DI-H_2O, and dried in a nitrogen stream. This leads to a deposit of densely packed ZnO nanorods, with a thickness of ~ 1 μm and an average nanorod diameter of ~ 75 nm. The nanorods are well-aligned perpendicular to the substrate surface.

2.1.1.2 VPT growth

The details of the VPT growth methods are as follows (more detail may be found in selected references).[2,24,25] Two methods of VPT growth were employed, one involving the seeded layers mentioned above, on Si substrates, and the other using an Au catalyzed vapour-liquid-solid (VLS) process to grow ZnO nanorods on sapphire substrates. For the case of VPT on seeded Si substrates, we have used two methods. Firstly, nanorods were grown by VPT directly through a hexagonal silica template onto CBD ZnO films (prepared using a slightly different method to that described above, based on forced hydrolysis of zinc acetate). The second method used an intermediate zinc acetate chemical bath deposition through a hexagonal silica template to initiate nanorod growth, followed by VPT. Equal masses of graphite and ZnO (0.06 g) were thoroughly mixed and placed in an alumina boat. Substrates were placed over this mixture with the seeded side facing the source powder. The boat was heated to 900^0C in a single zone horizontal tube furnace, with a 90 sccm Ar flow for 1 hour, and then cooled to room temperature. More detail on this VPT growth on seeded Si substrates is given in the references.[2] For the case of Au catalysed VLS-VPT three differently oriented sapphire substrates were utilised (c-plane (0001), a-plane (11-20) and r-plane (1-102)). Results below are shown only for samples on a-plane (11-20) substrates with a dense

coverage of well-aligned nanorods of mean length ~ 0.6 μm and mean diameter ~ 70 nm. Au catalyst was deposited on the substrates by sputtering to yield a 3 nm thick layer. ZnO powder was mixed with graphite powder and growth took place in a CVD furnace with a horizontal quartz tube. Ar was the inert carrier gas and the furnace was heated to 900ºC and the growths took 30 min. More detail on this VLS-VPT growth on sapphire substrates is given in the references.[24,25]

The fact that the morphologies and dimensions of the nanostructures grown by both CBD and VPT allows us to compare their optical behaviour without concerns that effects associated with different morphologies and/or dimensions would strongly affect the conclusions of our work.

The samples were structurally characterized by field emission SEM (FESEM; JEOL JSM-6400F and Hitachi H-4100FE) and x-ray diffraction (XRD; Bruker AXS D8 Advance Texture Diffractometer).

2.1.2 Linear and nonlinear optical characterisation

PL spectra were acquired using the 325 nm line of He-Cd laser with a Bomem Hartmann & Braun DA8 FT spectrometer with the samples in a closed cycle cryostat (Janis Research Co. Inc.). THG studies were carried with a Ti:sapphire laser (Venteon Femtosecond Laser Technologies), pumped by a frequency doubled Nd:YAG. The temporal width, repetition rate and energy of the original pulses from the laser were ~ 7 fs, 80 MHz and ~ 5.25 nJ, respectively. The central wavelength is ~ 810 nm and the spectral bandwidth, as determined by the full width at half maximum (FWHM), is > 300 nm. The laser was focussed for THG studies with a beam waist of ~ 4 μm, giving a peak intensity of ~ 1.5 x 10^{12} Wcm^{-2} in the case of the direct beam. iFROG measurements were made with a home-built system, using a Michelson interferometer configuration where one mirror is controlled by a piezoelectric controller (step size = 35 nm). Pulses from the two arms of the interferometer are recombined with varying delays and are focussed on the samples, as described above. The THG signal is separated, and residual pump radiation removed, by a THG reflecting mirror and an interference filter. The THG signal is analysed with an EMCCD-based spectrometer (Newton, Andor Technology, the EMCCD was cooled to -75^0C by a Peltier cooler). All THG experiments were carried out at room temperature. The interferometer mirror motion and the spectral data capture were synchronized using in-house LabView-based software. Further analysis of the iFROG data was performed using Femtosoft software (Femtosoft Technologies, FROG 3.0) following Fourier filtering which is used to extract normal frequency resolved optical gating (FROG) data.[20]

3.1 Experimental results and discussion

3.1.1 ZnO nanostructure growth and structural characterization

Figure 1 (a) shows 45^0 tilted-view FESEM data of the CBD grown deposit on fused silica, showing a densely packed ZnO nanorod film with a thickness of ~ 1 μm (and the inset shows a cross-sectional view) with an average nanorod diameter of ~ 75 nm. The nanorods are well-aligned normal to the substrate. Figure 1 (b) shows FESEM data for the VPT-grown ZnO

nanorod sample on sapphire. XRD data (not shown) confirm the crystalline ZnO phase in all cases.

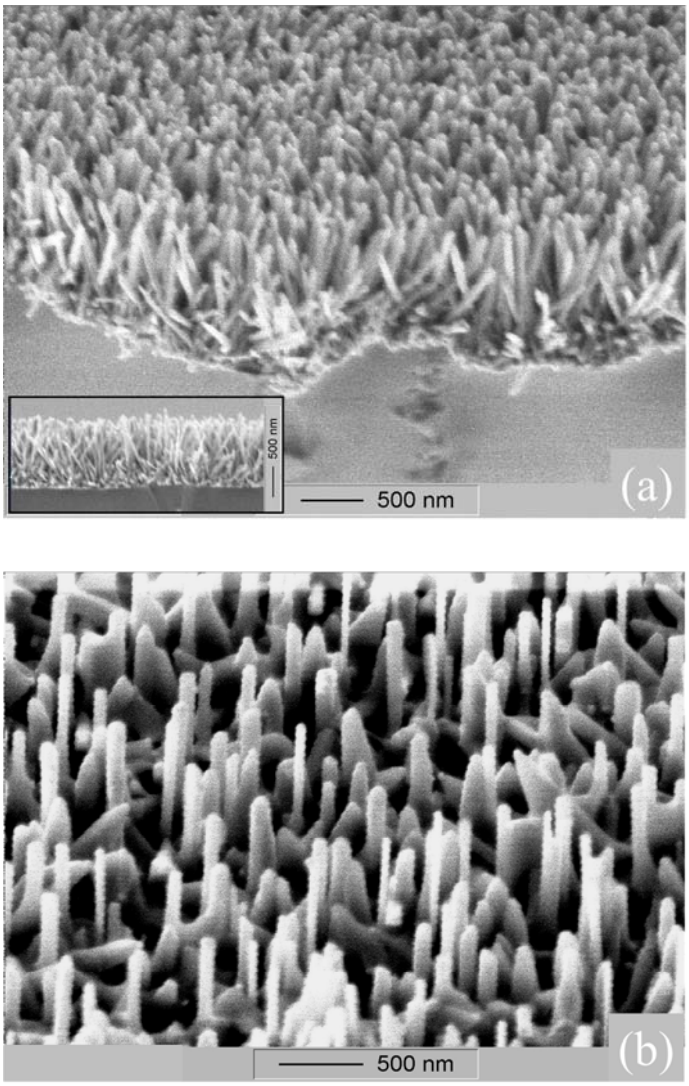

Fig. 1. (a) 45^0 tilted-view FESEM image of CBD-grown ZnO nanorod sample on fused silica (inset shows a cross-sectional view); (b) 45^0 tilted-view FESEM image of VPT-grown ZnO nanorod sample on a-plane sapphire

3.1.2 ZnO nanostructure linear and nonlinear optical characterisation

Figure 2 shows low temperature PL spectra for the CBD-grown (using forced hydrolysis of zinc acetate; samples grown by CBD using the NaOH method showed very weak and in some cases undetectable PL emission at low temperatures) and VPT-grown samples on Si substrates. Figures 2 (a) and (b) show data for different VPT-grown samples which both display strong emission and very narrow bound exciton linewidths. Various spectral features can be clearly resolved, including the I_2/SX, I_6 and I_9 lines (following the usual labelling).[26] The I_6 line at ~ 3.361 eV is present in all our VPT-grown samples due to Al impurities because the substrate and reaction mixture is placed in an alumina boat during

deposition.[26] The FWHM of this peak is ~ 0.5 meV indicating material of high quality. The I_9 line is found in the majority of samples and is ascribed to indium; the precise origin of indium is uncertain, but it is a common impurity in ZnO and may originate in the source powder or from growth system contamination.[27] An emission at ~ 3.367 eV is also observed in some samples, corresponding to the surface exciton (SX), assigned to surface adsorbed impurities.[28,29] The PL emission from CBD-grown material has also been measured, both with and without a final annealing step at 900^0C. The PL emission from the unannealed CBD-grown layer, shown in figure 2 (c), is extremely weak. After annealing, some improvement in the PL intensity was observed as shown in figure 2 (d). However the signal intensity is still ~ 100 times weaker than that from VPT-grown samples and the PL peak widths are far broader. Thus it is clear that the PL signal quality, in terms of intensity and spectral linewidth, is far poorer for the CBD-grown samples, compared to the VPT-grown samples. Before annealing the sole peak detected in the CBD-grown samples is a broad emission at ~ 3.368 eV, but after annealing this is replaced by a peak close to the I_9 position, supporting the assignment of the I_9 peak in VPT-grown samples to contamination of furnace equipment, as mentioned earlier.

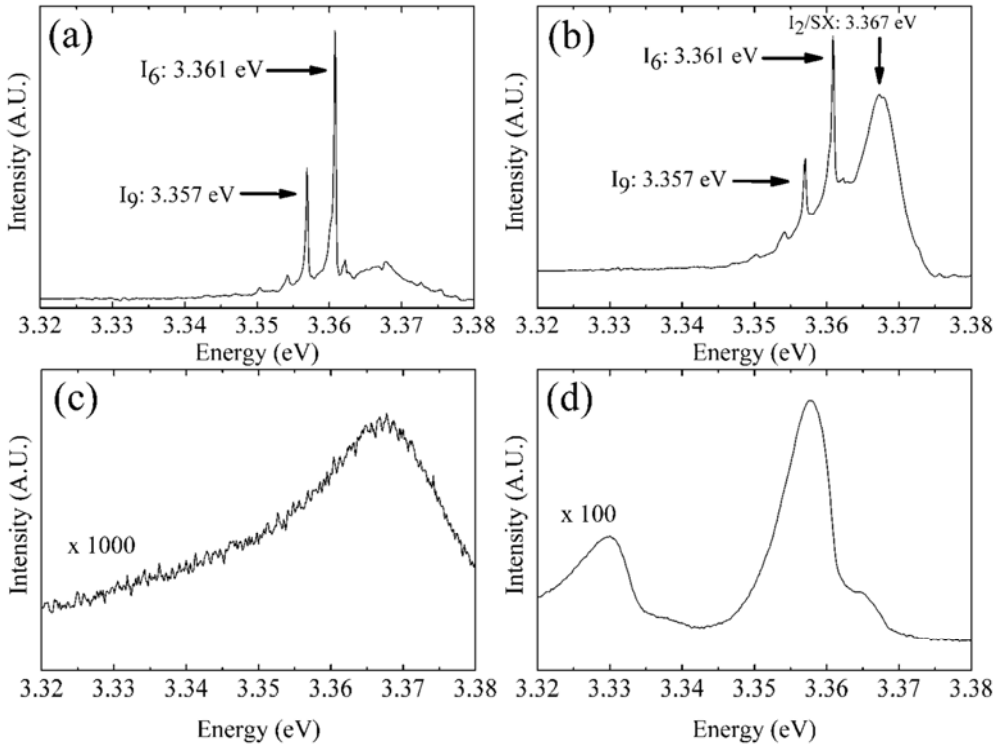

Fig. 2. PL emission at low temperature (~18-20K) from (a) and (b) VPT-grown ZnO nanorod samples on Si; (c) CBD-grown ZnO nanorod sample on Si without anneal; (d) CBD-grown ZnO nanorod sample on Si following 900^0C anneal. The y-axis intensities are comparable in all parts of the figure

Figure 3 (a) displays THG spectra for the CBD-grown sample on fused silica and the VPT-grown sample on a-plane sapphire under focused illumination by Ti:sapphire laser, with conditions as described earlier (the beam splitter in the iFROG set-up has fixed and unequal path lengths, leading to a pulse width of ~ 11 fs). Figure 3 (a) also shows surface enhanced THG (STHG) from a bare quartz surface, recorded under the exact same conditions. A signal

is seen at ~ 272 nm with bandwidth of ~ 20 nm from all samples, and this matches the expected spectral position for THG of the 810 nm fundamental laser very well.[30] The identification of this signal at 272 nm with THG is further evidenced by the dependence of its intensity on the exciting laser intensity, which is shown in figure 3 (b).

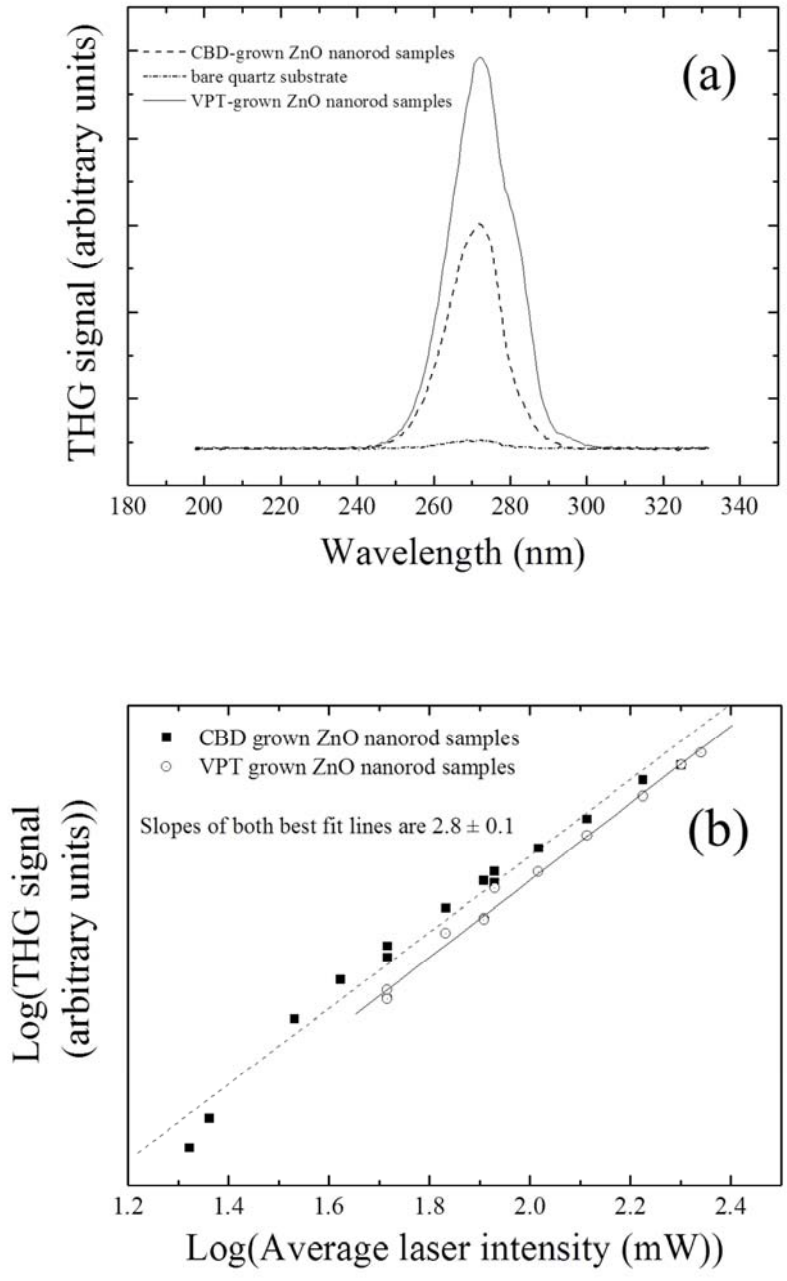

Fig. 3. (a) THG spectra for the CBD-grown (on fused silica) and VPT-grown (on a-plane sapphire) ZnO nanorod samples and for a bare quartz substrate, under focused laser excitation; (b) THG intensity variation as a function of exciting laser intensity for both the CBD- and VPT-grown ZnO nanorod samples

The exciting laser intensity was controlled using neutral density (ND) filters which cause temporal broadening of the pulse to ~ 42 fs (as well as chirp), and this causes a decrease in the peak intensity of the pulse. The broadening does not vary with the different ND filters used and the same laser pulse width was measured for beams which traversed different ND filter combinations, as shown in figure 5 below for a number of different combinations. The THG signal intensity from the CBD-grown and VPT-grown ZnO nanorod samples are comparable. In terms of the spectral details, the VPT-grown sample shows a small long wavelength shoulder, a feature also evident in iFROG data in figure 4 below, most likely due to different alignment and/or faceting of the ZnO nanostructures grown by CBD and VPT. It is known that nonlinear processes in nanostructures are often sensitive to the specific crystal termination.[31]

In figure 3 (b) the integrated 272 nm signal intensity (after baseline correction of THG intensity) is plotted versus laser intensity using log-log axes. The order of the nonlinear process should be given by the slope of this graph. For the case of both the CBD- and VPT-grown ZnO samples the slope is 2.8 ± 0.1, almost equal to the value of 3 expected for third order processes. The discrepancy from an exponent of 3 is very likely due to the deviation of the pulse temporal profile from an ideal “flat-top” profile, a feature which may decrease the measured values of the slopes slightly.

Clearly the THG efficiency of ZnO nanorod samples grown by both CBD and VPT is very similar, and in both cases is much greater than that associated with STHG at a bare quartz sample surface (at least one order of magnitude greater for the ZnO nanorod samples). The results from the characterisation of the nonlinear optical properties of the ZnO nanorod samples grown by both CBD and VPT thus differs very greatly from the characterisation results of the linear optical properties of ZnO nanorods grown by these two methods, as shown by the PL emission data in figure 2 above. The data in figure 2 show that PL from CBD-grown ZnO nanorods is always much weaker (and far broader spectrally) at low temperatures than that from VPT-grown ZnO nanorods.[2,3]

3.1.3 ZnO nanorods as frequency converters for third order pulse characterization with iFROG

iFROG data from CBD-grown and VPT-grown ZnO nanorod samples is shown in Figure 4 and the data from both sample types are very similar (noting the shoulder at longer wavelengths for the VPT-grown sample, mentioned earlier). Unprocessed THG iFROG data from the CBD- and VPT-grown samples is shown in 4 (a) and 4 (d), respectively. Fourier analysis of these data yields the various order frequency components; the DC and first order components are used to retrieve pulse shape using two independent approaches and thus iFROG allows an internal check on consistency, especially for delay axis calibration.[20,21,32] Our analysis concentrates on DC part of the data extracted by Fourier filtering and the resultant data are shown in Figures 4 (b) and 4 (e) (CBD- and VPT-grown ZnO nanorod samples, respectively). This data is the same as an ordinary FROG trace and can thus be processed directly by standard software for pulse retrieval. Here we have used commercial software (specified in the Experimental Details section) and the resultant spectral signal and spectral phase are given in Figures 4 (c) and 4 (f) (CBD- and VPT-grown ZnO

nanorod samples, respectively). The pulse duration is estimated at ~ 11 fs for the case of both CBD- and VPT-grown ZnO nanorod samples.

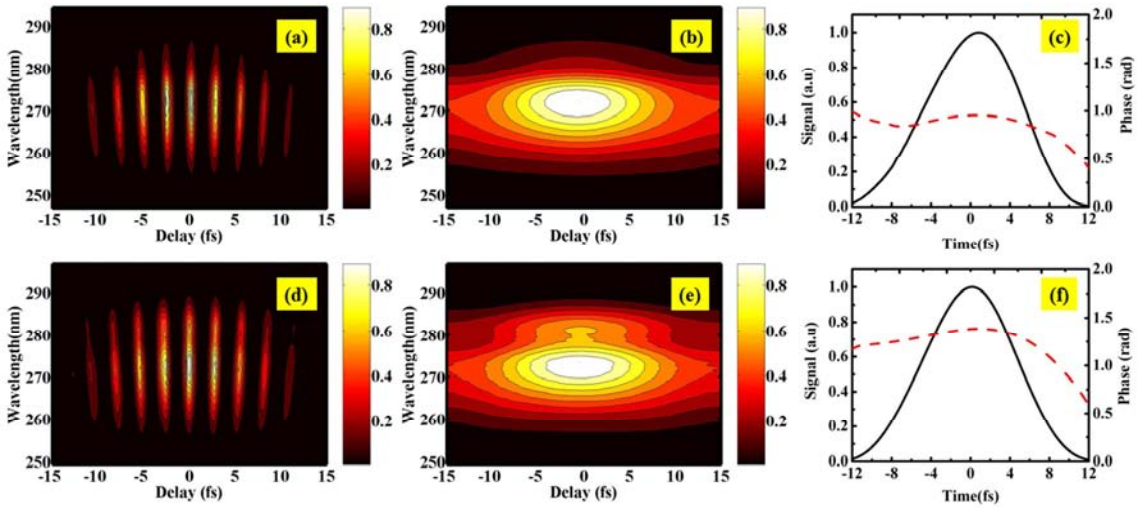

Fig. 4. (a) iFROG trace, (b) FROG and (c) temporal pulse profile of THG from ZnO CBD-grown nanorods; (d) iFROG trace, (e) FROG and (f) temporal pulse profile of THG from ZnO VPT-grown nanorods (no ND filter in beam path for any of these measurements)

The remaining nonlinear optical studies presented here are for the CBD-grown nanorod sample because data for VPT-grown samples are identical in all important respects. The time-bandwidth product from FROG analysis was 0.55. An unchirped Gaussian pulse has a time-bandwidth product of 0.44 and the larger product in the present case implies the presence of quadratic chirp; the curved phase profile in figure 4 (c) also clearly demonstrates this chirp which we attribute to the beam splitter of the iFROG system. This beam splitter has a quartz substrate of thickness 0.7 mm (from Venteon). The group delay dispersion (GDD) of this substrate is ~ 36 fs^2/mm and thus the net GDD (β_2) due to this beam splitter is 24 fs^2 (i.e. 36 fs^2/mm x 0.7 mm).[33,34] The pulse duration (τ) as a function of GDD is described by equation (1.1) below:

$$\tau = \tau_0 \sqrt{1 + \left(4 \cdot \ln(2) \cdot \left(\frac{\beta_2}{\tau_0^2} \right) \right)^2} \qquad (1.1)$$

In equation (1.1) τ_o = is the unchirped pulse duration (i.e. coming directly from the laser).[33–35] Inserting values for τ of 11 fs and for β_2 of 24 fs^2 into equation (1.1) yields a value for the unchirped pulse duration of τ_o = 7 fs, and this value is very close to the value measured by a commercial Few Cycle-Spectral Phase Interferometry for Direct Electric-field Reconstruction (FC-SPIDER; Applied Physics and Electronics – APE Ltd., Berlin, Germany) system of 6.7 fs. This excellent agreement shows the capability of CBD-grown ZnO nanorod samples to accurately recover values for initial pulse durations less than 10 fs.

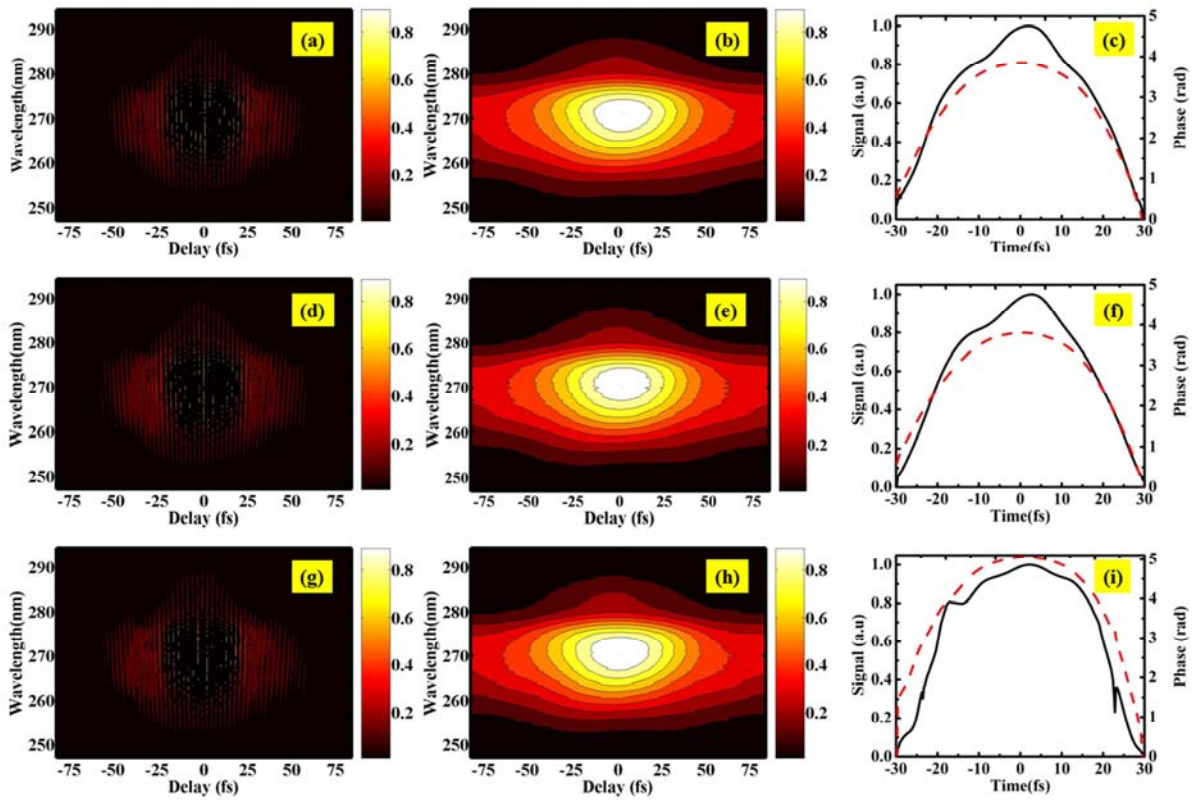

Fig. 5. iFROG trace, FROG and temporal pulse profile, respectively, for CBD-grown ZnO nanorods with ND filter optical density 0.04 + 0.04, (a), (b) and (c); with ND filter in path with with ND filter optical density 0.04 + 0.2, (d), (e) and (f); with ND filter in path with ND filter optical density 0.04 + 0.4, (g), (h) and (i)

In order to examine the pulse diagnostics capability of the ZnO nanorod sample under conditions of higher chirp we have measured the pulse parameters after the pulses have traversed highly dispersive (HD) optical materials. The HD optical materials employed are metal coated ND filters (New Focus, 2 filter wheel system), i.e. those previously employed for intensity variation studies shown in figure 2 above. We have used three different filtering conditions with quite different transmissions (i.e. ND values of 0.04 + 0.04, 0.04 + 0.2, 0.04 + 0.4; the two values are the ND optical densities of the two filters in the tandem set-up). Typical iFROG and DC component of iFROG (i.e. FROG) traces as well as pulse temporal profiles after traversing the ND filter combination are shown in Figures 5 (a) – (i), again for the CBD-grown nanorod sample. The duration of the pulse for all filtering combinations is essentially constant at ~ 42 fs. This increase in duration is caused by the very large chirp created by the ND filters. We have again used Femtosoft software to extract the spectral phase profile of the pulse (data not shown). Employing a standard Taylor series expansion of this phase profile gives a value for the GDD, β_2 of ~ 90 fs^2. By using this value in conjunction with the value for τ_o deduced from the analysis above (7 fs), we can compute the broadened pulse duration, using equation (1.1) again, to be ~ 38 fs, a value which is in excellent agreement with the experimentally observed pulse width of 42 fs.[33–35] The residual discrepancy between the computed and experimental values of ~ 4 fs is because equation (1.1) only includes second order chirp (GDD, which is normally the most important

term), but neglects third order dispersion (TOD) and higher order terms, and this explains the discrepancy.

4.1 Conclusions

This chapter has compared the linear and nonlinear optical properties of ZnO grown by CBD and VPT. Our data show that the linear optical properties of VPT-grown nanorods are vastly better, and PL emission from VPT-grown nanorods is very much more intense, as well as displaying much narrower excitonic linewidths at low temperatures. By contrast the nonlinear optical properties, such as THG, of the nanorods grown by the two methods are very similar and nanorods grown by methods are efficient sources for third harmonic UV generation. The THG signal has been studied using intensity dependence which clearly confirms the third order nonlinear nature of the spectral signal at ~ 272 nm. ZnO nanorod deposits give THG signals more than a factor of ten larger than STHG generated at a quartz sample surface. This demonstrates the material's suitability as an efficient UV generator using nonlinear up-conversion of red/near IR laser pulses. We have also reported iFROG studies of these ZnO nanorod samples, and have measured laser pulse parameters, as well as effects such as pulse broadening and chirping caused by ND filters utilised in certain configurations. This work clearly shows that ZnO nanorod deposits of this type can efficiently characterize laser pulses (of original durations < 10 fs).[36]

The efficiency of both CBD-grown and VPT-grown ZnO nanorods as third harmonic UV generation sources means that a number of growth methods, compatible with various substrates and with differing coverage and scalability capabilities, can be confidently used in future work to drive forward potential applications in iFROG characterization of ultrafast, few cycle, fs pulses as well as in biophysical studies of single cell UV irradiation.

5.1 Acknowledgments

EMcG, FG and RG acknowledge LaserLab Europe funding under project MBI001954 enabling travel by EMcG and FG to MBI for extended research visits. RG also acknowledges partial funding of the work by DFG grants (numbers GR1782-12-1 and GR1782-12-2). CG and EMcG acknowledge the Irish Research Council (IRC; formerly the Irish Research Council for Science, Engineering and Technology, IRCSET) for a postgraduate scholarship under the EMBARK initiative. DB and EMcG acknowledge support from Science Foundation Ireland via the Strategic Research Cluster grant entitled "Functional Oxides and Related Materials for Electronics" (FORME). Finally, we gratefully acknowledge T. Elsaesser and M. Tischer (both MBI) for essential support and stimulating discussions.

6.1 References

[1] Djurisic A B and Leung Y H 2006 Optical properties of ZnO nanostructures. *Small* **2** 944–61

[2] Byrne D, McGlynn E, Cullen J and Henry M O 2011 A catalyst-free and facile route to periodically ordered and c-axis aligned ZnO nanorod arrays on diverse substrates. *Nanoscale* **3** 1675–82

[3] McGlynn E, Henry M O and Mosnier J-P 2009 ZnO wide bandgap semiconductor nanostructures: growth, characterisation and applications *Handbook of Nanoscience and Technology vol. II* ed A V Narlikar and Y Y Fu (Oxford: Oxford University Press) pp 575–624

[4] Greene L E, Law M, Tan D H, Montano M, Goldberger J, Somorjai G and Yang P 2005 General route to vertical ZnO nanowire arrays using textured ZnO seeds. *Nano Lett.* **5** 1231–6

[5] Postels B, Kreye M, Wehmann H H, Bakin A, Boukos N, Travlos A and Waag A 2007 Selective growth of ZnO nanorods in aqueous solution *Superlattices Microstruct.* **42** 425–30

[6] Bai W, Yu K, Zhang Q X, Zhu X, Peng D Y, Zhu Z Q, Dai N and Sun Y 2008 Large-scale synthesis of zinc oxide rose-like structures and their optical properties *Phys. E-Low-Dimensional Syst. Nanostructures* **40** 822–7

[7] Bekeny C, Voss T, Gafsi H, Gutowski J, Postels B, Kreye M and Waag A 2006 Origin of the near-band-edge photoluminescence emission in aqueous chemically grown ZnO nanorods *J. Appl. Phys.* **100** 104317

[8] Grabowska J, Meaney A, Nanda K, Mosnier J-P, Henry M, Duclère J-R and McGlynn E 2005 Surface excitonic emission and quenching effects in ZnO nanowire/nanowall systems: Limiting effects on device potential *Phys. Rev. B* **71** 115439

[9] Petrov G I, Shcheslavskiy V, Yakovlev V V, Ozerov I, Chelnokov E and Marine W 2003 Efficient third-harmonic generation in a thin nanocrystalline film of ZnO *Appl. Phys. Lett.* **83** 3993–5

[10] Wang K, Zhou J, Yuan L, Tao Y, Chen J, Lu P and Wang Z L 2012 Anisotropic third-order optical nonlinearity of a single ZnO micro/nanowire. *Nano Lett.* **12** 833–8

[11] Das S K, Bock M, O'Neill C, Grunwald R, Lee K M, Lee H W, Lee S and Rotermund F 2008 Efficient second harmonic generation in ZnO nanorod arrays with broadband ultrashort pulses *Appl. Phys. Lett.* **93** 181112

[12] Pedersen K, Fisker C and Pedersen T G 2008 Second-harmonic generation from ZnO nanowires *Phys. status solidi* **5** 2671–4

[13] Kobayashi Y, Yoshitomi D, Iwata K, Takada H and Torizuka K 2007 Ultrashort pulse characterization by ultra-thin ZnO, GaN, and AlN crystals. *Opt. Express* **15** 9748–54

[14] Das S K, Schwanke C, Pfuch A, Seeber W, Bock M, Steinmeyer G, Elsaesser T and Grunwald R 2011 Highly efficient THG in TiO2 nanolayers for third-order pulse characterization *Opt. Express* **19** 16985–95

[15] Zhang C, Zhang F, Qian S, Kumar N, Hahm J and Xu J 2008 Multiphoton absorption induced amplified spontaneous emission from biocatalyst-synthesized ZnO nanorods *Appl. Phys. Lett.* **92** 233116

[16] Sridhar D, Xie J N, Abraham J K and Varadan V K 2007 Synthesis arid photonic property study of ZnO nanowires for a real time photodynamic therapy monitoring probe *Nanosensors, Microsens. Biosens. Syst. 2007* **6528** L5281–L5281 510

[17] Baratto C, Comini E, Faglia G, Sberveglieri G, Zha M and Zappettini A 2005 Metal oxide nanocrystals for gas sensing *Sensors Actuators, B Chem.* **109** 2–6

[18] Li J, Guo D, Wang X, Wang H, Jiang H and Chen B 2010 The Photodynamic Effect of Different Size ZnO Nanoparticles on Cancer Cell Proliferation In Vitro. *Nanoscale Res. Lett.* **5** 1063–71

[19] Al-Hilli S M, Willander M, Öst A and Strålfors P 2007 ZnO nanorods as an intracellular sensor for pH measurements *J. Appl. Phys.* **102** 084304

[20] Stibenz G and Steinmeyer G 2005 Interferometric frequency-resolved optical gating. *Opt. Express* **13** 2617–26

[21] Stibenz G and Steinmeyer G 2006 Structures of interferometric frequency-resolved optical gating *IEEE J. Sel. Top. Quantum Electron.* **12** 286–96

[22] Byrne D, McGlynn E, Kumar K, Biswas M, Henry M O and Hughes G 2010 A Study of Drop-Coated and Chemical Bath-Deposited Buffer Layers for Vapor Phase Deposition of Large Area, Aligned, Zinc Oxide Nanorod Arrays *Cryst. Growth Des.* **10** 2400–8

[23] Byrne D, McGlynn E, Henry M O, Kumar K and Hughes G 2010 A novel, substrate independent three-step process for the growth of uniform ZnO nanorod arrays *Thin Solid Films* **518** 4489–92

[24] Güell F, Ossó J O, Goñi A R, Cornet A and Morante J R 2009 Synthesis and optical spectroscopy of ZnO nanowires *Superlattices Microstruct.* **45** 271–6

[25] Güell F, Ossó J O, Goñi A R, Cornet A and Morante J R 2009 Direct imaging of the visible emission bands from individual ZnO nanowires by near-field optical spectroscopy. *Nanotechnology* **20** 315701

[26] Meyer B K, Alves H, Hofmann D M, Kriegseis W, Forster D, Bertram F, Christen J, Hoffmann a., Straßburg M, Dworzak M, Haboeck U and Rodina a. V. 2004 Bound exciton and donor–acceptor pair recombinations in ZnO *Phys. Status Solidi* **241** 231–60

[27] Strassburg M, Rodina A, Dworzak M, Haboeck U, Krestnikov I L, Hoffmann A, Gelhausen O, Phillips M R, Alves H R, Zeuner A, Hofmann D M and Meyer B K 2004 Identification of bound exciton complexes in ZnO *Phys. status solidi* **241** 607–11

[28] Biswas M 2010 *PhD Thesis: Growth and Characterisation of ZnO Nanostructures: Excitonic Properties and Morphology* (Dublin City University. School of Physical Sciences)

[29] Biswas M, Jung Y S, Kim H K, Kumar K, Hughes G J, Newcomb S, Henry M O and McGlynn E 2011 Microscopic origins of the surface exciton photoluminescence peak in ZnO nanostructures *Phys. Rev. B* **83** 235320

[30] Tsang T 1995 Optical third-harmonic generation at interfaces *Phys. Rev. A* **52** 4116–25

[31] Neumann U, Grunwald R, Griebner U, Steinmeyer G, Schmidbauer M and Seeber W 2005 Second-harmonic performance of a-axis-oriented ZnO nanolayers on sapphire substrates *Appl. Phys. Lett.* **87** 171108

[32] Anderson A, Deryckx K S, Xu X G, Steinmeyer G and Raschke M B 2010 Few-femtosecond plasmon dephasing of a single metallic nanostructure from optical response function reconstruction by interferometric frequency resolved optical gating. *Nano Lett.* **10** 2519–24

[33] Marcuse D 1980 Pulse distortion in single-mode fibers *Appl. Opt.* **19** 1653–60

[34] Walmsley I, Waxer L and Dorrer C 2001 The role of dispersion in ultrafast optics *Rev. Sci. Instrum.* **72** 1–29

[35] RP Photonics Webpages - chromatic dispersion *http://www.rp-photonics.com/chromatic_dispersion.html*

[36] Das S K, Güell F, Gray C, Das P K, Grunwald R and McGlynn E 2014 ZnO nanorods for efficient third harmonic UV generation *Opt. Mater. Express* **4** 701–9